



Nanofibrous mat-enabled soil water absorption for continuous soil nitrate sensing

Vignesh Kumar Thoomatti Haridass^{a,b}, Michael J Castellano^c, Liang Dong^{a,b,*}

^a Department of Electrical and Computer Engineering, Iowa State University, Ames, IA 50011, United States

^b Microelectronics Research Center, Iowa State University, Ames, IA 50011, United States

^c Department of Agronomy, Iowa State University, Ames, IA 50011, United States

ARTICLE INFO

Keywords:

Nanofibrous mat
Soil sensor
Nitrate
Electrospinning
Precision agriculture

ABSTRACT

Continuous monitoring of soil nitrate levels is essential for effective soil nutrient management. However, limited soil pore water at low soil water content levels hinders miniaturized soil sensor surfaces from efficiently interacting with nutrient ions. To address this, we introduce a nanofibrous mat designed to enhance nitrate detection by increasing connectivity between miniature sensors and the soil solution. Composed of polysulfone, polymethylmethacrylate, and polyvinyl alcohol, this mat is fabricated using electrospinning and electro-spray methods to balance water absorbency, mechanical durability, and ease of manufacturing. When wrapped around an ion-selective electrode-based nitrate sensor, the mat improves access to soil pore water, acts as a filter, prevents direct sensor-soil particle contact, and reduces the impact of soil particle surface charges on sensor measurements. Continuous nitrate monitoring with both mat-wrapped and bare sensors was conducted in controlled and field environments. Linear regression analysis indicates that the mat-wrapped sensor has a stronger correlation with conventional salt extract methods for measuring soil nitrate levels. T-tests confirm statistically significant differences between sensor measurements and the salt extraction method. Additionally, Bland-Altman analysis reveals that mat-wrapping reduces mean bias and narrows the limits of agreement, demonstrating improved agreement with the conventional method. Notably, the mat-wrapped sensor performs consistently across varying soil moisture conditions. These findings suggest that the water-absorbing mat improves the ability of the sensor to monitor nitrate continuously by accommodating varying soil moisture levels over time, making the mat-wrapped soil nitrate sensor a viable improvement for in-field measurements of soil solution chemistry.

1. Introduction

Soil nitrogen (N) is essential for plant growth and external inputs of N fertilizer are required for crop production. However, determining the optimal amount of N fertilizer input is challenging because the soil naturally provides a large, but highly uncertain, amount of N in the form of nitrate (NO_3^-) (Bowles et al., 2018). Greater certainty about how much nitrate the soil provides before and during crop growth would improve yields and environmental outcomes. One solution is to use inexpensive soil nitrate sensors to obtain real-time data on soil nitrate levels. Soil nitrate levels, measured with conventional methods, are well known to aid decision-making for agricultural management (Ali et al., 2019; Baumbauer et al., 2022; Chen et al., 2024; Fan et al., 2022; Grell et al., 2021). However, continuous soil nitrate sensors offer significant

advantages over conventional methods because conventional methods are costly, time-consuming, and do not provide real-time information. Therefore, there is a growing demand for low-cost, accurate, continuous soil nitrate sensors to enhance agricultural management practices.

Several low-cost soil nitrate sensing methods have been developed, including electrochemical sensors (Essoussi et al., 2019; Sookhajian et al., 2021), microfluidic-chip sensors (Khanfar et al., 2017; Murphy et al., 2021), and ion-selective electrodes (ISE) (Ali et al., 2019; Chen et al., 2024; Fan et al., 2022; Zhu et al., 2021). While many electrochemical sensors utilize ion-specific enzymes for molecular recognition, their long-term performance can be affected by enzyme stability (Ahmad et al., 2017). Microfluidic chips, which integrate electrophoretic separation mechanisms and electrochemical sensors, have been designed to measure multiple ions in soil water simultaneously but face

* Corresponding author.

E-mail address: ldong@iastate.edu (L. Dong).

<https://doi.org/10.1016/j.compag.2025.110319>

Received 25 October 2024; Received in revised form 16 March 2025; Accepted 18 March 2025

Available online 23 March 2025

0168-1699/© 2025 Elsevier B.V. All rights reserved, including those for text and data mining, AI training, and similar technologies.

challenges in extracting soil water for continuous measurement (Kung et al., 2019; Xu et al., 2017). ISE sensors have gained considerable attention due to their simple structure, rapid response, and compact size. Significant efforts have been made to address issues such as potential drift, interference from non-target species in the soil (Chen et al., 2021; Shishkanova et al., 2011), biofouling of ion-selective membranes (ISM) (Szigeti et al., 2006), inconsistency in sensor production, and instability of pseudo-reference electrodes (Hu et al., 2016). Essentially, ISE sensors operate on the principle of equilibrium concentration between the ISE surface and the surrounding solution, requiring both reference and working electrodes to be exposed to liquid solutions or wet environments (Jackson and Nelson 2019; Zdrachek and Bakker 2018). However, a notable challenge with deployment of ISM materials in soils is that they generally possess hydrophobic properties that repel aqueous solutions, hindering the movement of target ions into the membrane (Chen et al., 2024; Fan et al., 2022). This issue is exacerbated when soil moisture levels are low. The mixed solid-gas-solution composition of soil leads to inconsistent interaction between the sensor and soil solution, leading to inaccurate and inconsistent measurements over time.

To solve this issue, several methods have been suggested to draw soil pore water, thereby bringing mobile ions into contact with the sensor surface (Bieg et al., 2017; Wang et al., 2022). For example, surface modification techniques using self-assembled functional groups like $-\text{COOH}$, $-\text{OH}$, and $-\text{NH}_2$ can create a hydrophilic sensor surface. Similarly, other treatments, such as plasma treatment with ultraviolet and ozone, allow for enhancing wettability by increasing the presence of

$-\text{OH}$ groups. Another approach involves depositing metal oxide nanoparticles onto the sensor surface. Despite these efforts, nitrate sensors still face significant instability and unreliability when soil water content decreases (Chen et al., 2024). A recent, promising method involves coating the sensor surface with a thin hydrogel layer and a hydrophilic polyvinylidene fluoride (PVDF) layer to facilitate ion transport from the soil to the sensor surface (Chen et al., 2024; Fan et al., 2022). However, a drawback of using hydrogel is mechanical weakness, which compromises the durability and structural integrity of the sensor (Hu et al., 2023; Sun et al., 2020). Additionally, the ability of hydrophilic PVDF to promote long-term nitrate measurements under field conditions remains unknown (Chen et al., 2024).

This paper presents a nanofibrous mat designed to enhance soil water absorption, improving the performance of an ISE-based nitrate sensor. By drawing soil pore water toward the sensor surface, the mat increases surface wetness, ensuring connectivity between the sensor surface and the soil water for continuous nitrate detection (Fig. 1). Its high hydrophilicity and efficient water absorption overcome a common challenge faced by many miniaturized soil nitrate sensors, which often perform poorly under low soil moisture conditions due to limited interaction with nutrient ions in soil pore water. The mat ensures consistent ion detection across varying soil moisture levels. Furthermore, its enhanced mechanical strength prevents the sensor from potential damage caused by direct contact with soil particles. The porous structure of the mat also acts as a filter, allowing soil water to reach the sensor while reducing the impact of surface charges from soil particles on the sensor output. This

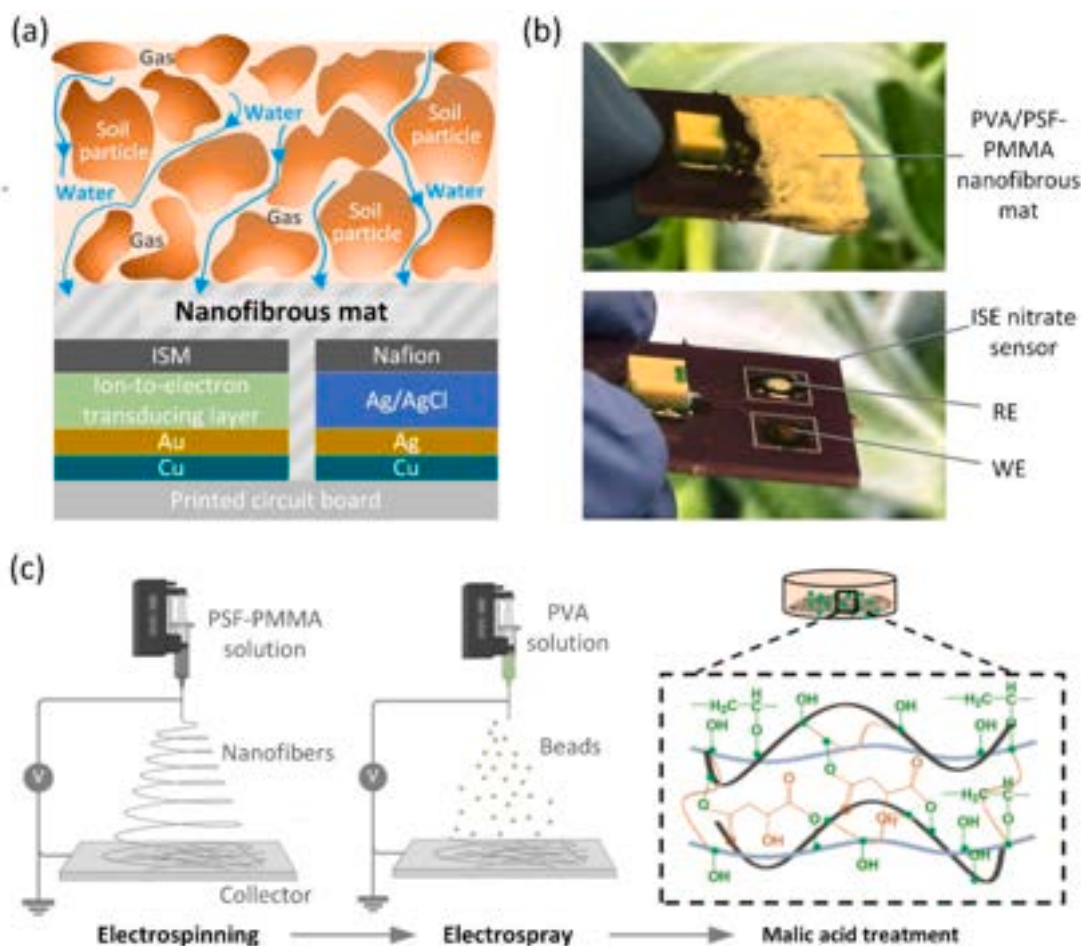


Fig. 1. (a) Schematic of an ISE-based nitrate sensor incorporated with a nanofibrous mat to enhance soil water absorption and interaction with the sensor surface. (b) Photographs of the PVA/PSF-PMMA mat-wrapped nitrate sensor in the upper panel and the bare sensor without the mat in the lower panel. (c) Preparation of the PVA/PSF-PMMA nanofibers through the electrospinning of PSF-PMMA nanofibers, electro spray of PVA beads, and malic acid treatment to enable cross-linking of PVA with PSF-PMMA.

nanofibrous mat enables more reliable and robust soil nitrate sensing across diverse soil moisture conditions.

2. Experimental

2.1. Nanofibrous mat design

The nanofibrous mat was composed of polysulfone (PSF), polymethylmethacrylate (PMMA), and polyvinyl alcohol (PVA) and was formed through a combination of electrospinning and electrospray (Huang et al., 2022) techniques (Fig. 1c). Initially, PSF-PMMA nanofibers were produced via electrospinning, and then PVA was applied to the PSF-PMMA nanofiber surface through electrospray, followed by using a cross-linking method to stabilize the PVA on the surface of the PSF-PMMA nanofibers. The design of this mat balanced water absorptency, mechanical durability, and ease of manufacturing. Specifically, PSF provided high mechanical strength, fouling resistance, and thermal and chemical stability (Chee et al., 2022). However, due to poor electrospinnability, PSF nanofibers tended to agglomerate (Obaid et al., 2015). This issue was mitigated by incorporating PMMA, which improved the electrospinnability of the PSF-PMMA nanofibers (Wu et al., 2022; Xu et al., 2018). The hydrophobic nature of PSF-PMMA nanofibers, however, impeded soil water absorption, a crucial drawback addressed by coating the nanofibers with hydrophilic PVA (Park et al., 2018). Directly blending PVA with the PSF-PMMA precursor solution for electrospinning would result in phase separation due to the incompatibility between the hydrophobic characteristics of PSF-PMMA and the hydrophilic characteristics of PVA (Li et al., 2020). Therefore, PVA was electrosprayed onto the PSF-PMMA nanofibers. To ensure the stability of PVA in soil water, the PVA-coated PSF-PMMA (or PVA/PSF-PMMA) nanofibers were treated with a malic acid solution. This treatment facilitated cross-linking between the carboxylic groups of malic acid and the hydroxyl groups of PVA (Valdés et al., 2021) thus stabilizing the PVA/PSF-PMMA nanofibrous mat in water.

2.2. ISE sensor manufacturing

The manufacturing method of the ISE nitrate sensor used in this study (Fig. 1a) is detailed in our previous work (Ali et al., 2019). Briefly, the sensor comprised a working electrode (WE; 2.5 mm diameter) and a reference electrode (RE; 2.5 mm diameter) on a printed circuit board (PCB). The conducting base electrodes and wires of the sensor were made of copper on the PCB. The WE consisted of a 10 nm-thick titanium (Ti) layer, a 250 nm-thick gold (Au) layer, a nanocomposite of poly(3-octyl-thiophene) (POT), and molybdenum disulfide (MoS_2) serving as an ion-to-electron transducing layer, and an ISM for nitrate selection (Ali et al., 2019). To prepare the POT- MoS_2 nanocomposite, 2.6 mg of POT was dissolved in 1 mL of tetrahydrofuran (THF) solvent. Then, 10.4 mg of MoS_2 was added. The mixture was sonicated for 4 h to achieve a uniform dispersion. The NO_3^- -ISM was prepared by mixing the following components, including 1.50 wt% of tridodecylmethylammonium nitrate, 5.75 wt% of polyvinyl chloride, 16.25 wt% of 2-nitrophenyl octyl ether, 0.25 wt% of methyltriphenylphosphonium bromide, 1.93 wt% of nitrocellulose (moistened with 2-propanol), and 74.3 wt% of THF. The mixture was stirred at 1500 rpm and 30 °C for 12 h to obtain a homogeneous solution (Ali et al., 2019). The RE consisted of a 500 nm-thick silver (Ag) layer, a 500 μm -thick Ag/AgCl paste layer, and an 80 nm-thick protonated Nafion layer to minimize chloride ion leaching to the surrounding environment. Waterproof epoxy covered the device, exposing the WE and RE to the soil. Before use, the sensor was pre-conditioned by immersion in a 2500 ppm NO_3^- solution for 24 h (Zhu et al., 2021).

2.3. Formation of PVA/PSF-PMMA nanofibers

Initially, a mixture solution of PSF-PMMA was prepared by

dissolving 1.2 g PSF pellets (Sigma-Aldrich; MO, USA) and 0.3 g PMMA powder (Sigma-Aldrich; MO, USA) in 8.5 mL N, N-dimethylformamide (DMF; Sigma-Aldrich; MO, USA). This mixture was stirred at 1100 rpm and 60 °C for 12 h to obtain homogeneous dissolution. Subsequently, for the electrospinning of PSF-PMMA nanofibers, a 27 kV DC voltage (Gamma High Voltage Research, FL, USA) was applied between a metal spinneret and a fiber collector (Fig. 1c). The spinneret consisted of a blunt-end metal needle with an inner diameter of 0.84 mm and an outer diameter of 1.27 mm (gage size: 18G; Nordson EFD, OH, USA). The fiber collector was a stainless flat plate (15.3 × 12.7 cm) covered with 1 mm thick aluminum foil (Reynolds Wrap, IL, USA). The spinneret-to-collector distance was set at 10 cm. The polymer mixture solution of PSF-PMMA was loaded into a 10 mL syringe driven by a syringe pump (catalog #14-831-200; Fisher Scientific, NH, USA) at a feed rate of 1.5 mL/h. During electrospinning, the electric field stretched the polymer solution into elongated fibers, which were then deposited onto the collector as PSF-PMMA nanofibers.

To electrospray PVA on the PSF-PMMA nanofibers, a PVA solution was prepared by dissolving 1.2 g PVA (Sigma-Aldrich, MO, USA) in 8.8 mL dimethylsulfoxide (DMSO; Sigma-Aldrich; MO, USA) and stirring the mixture at 1100 rpm at 70 °C for 2 h to achieve a homogeneous solution. This solution was then electrosprayed onto the PSF-PMMA nanofibers using the same setup and conditions as described for the electrospinning process. However, unlike the nanofiber formation observed with electrospinning, the PVA solution formed droplets (Fig. 1c) due to the higher boiling point of DMSO (189 °C), which limited solvent evaporation during the process. To ensure complete evaporation of the DMSO from the PVA droplets, the PVA-coated PSF-PMMA mat was placed in a vacuum-drying oven at 90 °C for 8 h. After that, the dried mat was wrapped around the ISE sensor. The sensor with the mat was immersed in a 1 % crosslinker solution of malic acid (MA; Sigma-Aldrich; MO, USA) for 12 h (Fig. 1c). Finally, the sensor was rinsed with deionized water to remove residual solvents.

2.4. Fiber characterization

Surface morphology of the pristine PSF, PSF-PMMA, and PVA/PSF-PMMA nanofibers were examined using a scanning electron microscope (FEI Quanta-FEG 250, OR, USA). Attenuated total reflectance-Fourier transform infrared (ATR-FTIR) spectroscopy (Bruker Tensor 37, MA, USA) was used to examine the surface functionalities of these nanofibers. Additionally, the hydrophilicity of these nanofibers was evaluated by measuring their water contact angles on a homemade goniometer.

2.5. Sensor characterization using treated soils

Sensor characterizations were conducted using soil collected from the Iowa State University Agronomy and Agricultural Engineering Research Farm. The soils were washed, air-dried, and sterilized in a muffle furnace at 400 °C to reduce microbial activity (Zhu et al., 2021). The sterilized soil was then adjusted to a bulk density of 1.25 g cm^{-3} and prepared with three gravimetric soil water contents (0.2, 0.3, and 0.4 g/g) and five soil solution NO_3^- concentrations (10, 25, 50, 75, and 100 mg/L). These gravimetric soil water contents and NO_3^- concentrations were chosen because they encompass the typical ranges observed during the growing season in the rainfed Corn Belt maize fields (Zhu et al., 2021). Each sensor was installed in the center of each cup for measurements.

2.6. Field study

Field studies were conducted to assess the performance of mat-wrapped and bare ISE sensors. These devices were deployed at two adjacent locations (~40 cm apart) at the Iowa State University Agronomy and Agricultural Engineering Research Farm. Both types of

sensors were placed approximately 25 cm beneath the surface soil at each location. Sensor readings (measured in mV) were recorded at 20-minute intervals from September 17 to October 11, 2023. Sensors were considered functional when the difference between the pre- and post-deployment calibration curves was less than 20 % (Zhu et al., 2021).

To obtain ground-truth nitrate levels in the soil, samples were collected from locations close to the installed sensors and analyzed using the salt extract method (Zhu et al., 2021). These samples were mixed with 2 M KCl solution (1:5 soil-to-solution ratio) and shaken reciprocally for 1 h at 180 rpm. The soil slurry was then filtered using Whatman #1 filter paper, and the filtrates were refrigerated until analysis. The NO_3^- concentrations (mg/L) of the filtrates were measured with colorimetry in microplates using the Griess–Ilosvay reaction with VCl_3 as a reagent (Zhu et al., 2021).

To convert the NO_3^- concentration in the filtrate (mg/L of) to mg/kg of dry soil, the gravimetric soil water content was first calculated using the equation: Gravimetric soil water content (g/g) = [Weight of wet soil (g) – Weight of oven-dried soil (g)] / Weight of oven-dried soil (g) (Hack, 1984) and then the conversion was completed using the equation (Zhu et al., 2021): NO_3^- (mg/L) soil solution \times gravimetric soil water content (g/g) = NO_3^- (mg/kg) of dry soil.

3. Results and discussion

3.1. Material characterization

Fig. 2a shows the surface morphology of PSF nanofibers, which were aggregated during electrospinning due to intermolecular hydrogen bonding between PSF molecules. For the PSF-PMMA nanofibers, the microstructure of the PSF matrix transforms because PMMA was dispersed throughout the PSF matrix, reducing the opportunities for intermolecular hydrogen bonding between PSF molecules. This disruption minimized the tendency of PSF molecules to aggregate during electrospinning (Fig. 2b). Additionally, electrospayed PVA beads were used to modify the PSF-PMMA (Fig. 2c). The formation of the PVA beads instead of fibers was associated with the slow evaporation of the DMSO solvent. DMSO has a high boiling point, making it difficult to evaporate completely during the electrospaying process. When the solvent evaporated slowly, the polymer solution remained in a more liquid state for a longer period, preventing the formation of continuous fibers. Instead, the solution tended to form droplets, which solidified into beads as the solvent gradually evaporated.

The water contact angle measurement (Fig. 2d–2f) showed that the PSF and PSF-PMMA nanofibers exhibited a similar contact angle of $\sim 84^\circ$. However, the surface modification with sprayed PVA significantly reduced the contact angles to nearly zero, indicating enhanced

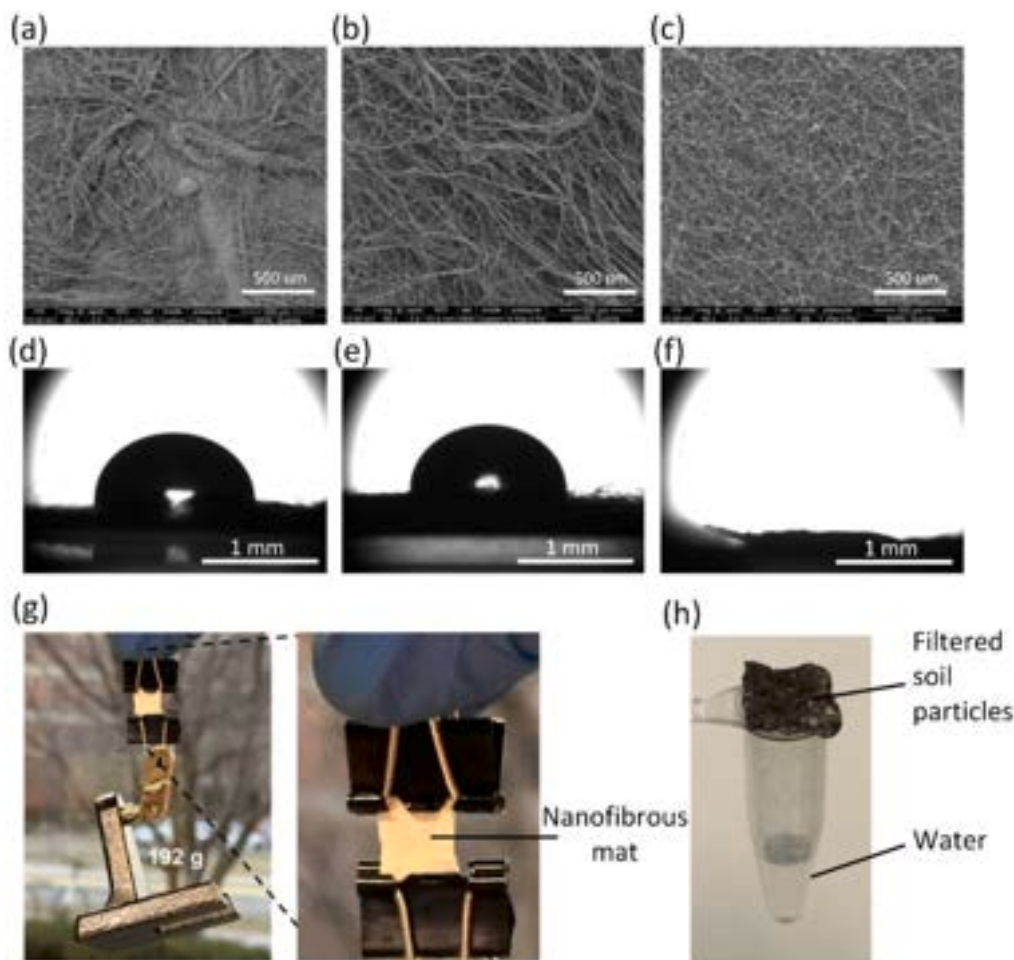


Fig. 2. (a)–(c) SEM images of electrospun PSF nanofibers (a), electrospun PSF-PMMA nanofibers (b), and PVA/PSF-PMMA mat formed by electrospaying PVA beads onto the PSF-PMMA nanofibers (c). (d)–(f) Optical images of water-contact angles at the surfaces of PSF nanofibers (d), PSF-PMMA nanofibers (e), and PVA/PSF-PMMA mat (f). (g) A PVA/PSF-PMMA mat with dimensions of 1.2 cm \times 1.0 cm \times 275 μm (length \times width \times thickness) clamped by two clips, lifting a 192 g metal piece. (h) Soil particles filtered and remained on a PVA/PSF-PMMA mat (275 μm thickness) affixed to the opening of a vial after a mixture of soil and water was loaded onto the mat.

hydrophilicity. This improvement was attributed to the presence of water-soluble -OH groups in PVA. Additionally, to demonstrate the high mechanical strength, the mat was clamped on both sides using a paper clip and tested by lifting a 192 g iron base of a soldering welding stand. The mat maintained its integrity during the test (Fig. 2g). Further, the mat was capable of filtering water from a soil-mixed water sample. In this experiment, a mixture of soil and water was gradually loaded onto the mat affixed to the opening of a vial. Most soil particles were filtered out and remained on the mat, while the water infiltrated into the vial (Fig. 2h).

Fig. 3 shows the FTIR spectra of the pristine PSF, PSF-PMMA, and PVA/PSF-PMMA nanofibers. The peaks at 633 and 696 cm^{-1} indicated the stretching vibrations of C-O and C-S bonds, respectively. Additionally, the peaks at 1148, 1237, and 1323 cm^{-1} were associated with the sulfonyl group (O=S=O), while the peak at 1295 cm^{-1} indicated the presence of the aromatic ether group (C-O-C) (Sadare and Daramola 2021). The peaks observed in the 832–873 cm^{-1} range were associated with the stretching vibrations of C=C bonds within the aromatic ring structure (Fig. 3a). Also, the peak in the 2869–2998 cm^{-1} range was attributed to the stretching of C-H bonds in alkane moieties (Fig. 3b). Furthermore, compared to the pristine PSF, a new peak appeared at 1729 cm^{-1} for PSF-PMMA and PVA/PSF-PMMA, indicating the stretching vibration of -COOCH₃ in PMMA (Fig. 3a). The broad band observed at 3406 cm^{-1} in the PVA/PSF-PMMA spectra (Fig. 3b) was due to the stretching vibration of O-H in PVA, confirming that PVA was successfully coated on the PSF-PMMA nanofibers by the electrospray process.

The water absorption study for the PVA/PSF-PMMA nanofibrous mat was conducted to assess the capacity of the mat to absorb water. Initially, the mat was weighed in its dry state and then immersed in 20 mL of deionized water for 24 h at room temperature. After soaking, the mat was reweighed, and the weight difference was used to calculate the amount of water absorbed (Sim et al., 2023). A 0.1 g dry mat absorbed approximately 0.1 g of water, confirming its considerable water absorption capability.

To evaluate the ion sorption capacity of the mat, five identical 0.1 g dry mats were individually immersed in 20 mL nitrate solutions with concentrations of 10, 25, 50, 75, and 100 ppm, respectively. The mats were left in immersion for 24 h at room temperature to ensure sufficient interaction with nitrate ions (Mohammad and Atassi 2020). After that, the remaining nitrate concentrations in the solutions were measured using a spectrophotometer.

The equilibrium adsorption isotherms for nitrate adsorption onto the nanofibrous mats were analyzed using the Langmuir and Freundlich isotherm models (Santos et al., 2020; Song et al., 2016). Fig. 4 illustrates the adsorption isotherms, demonstrating the adsorption capacity and

surface interactions between the mats and nitrate ions. The Langmuir model was applied to study the monolayer sorption of nitrate ions on the mat surface. The linearized Langmuir model is represented by Equation (1) (Santos et al., 2020; Song et al., 2016):

$$\frac{C_e}{q_e} = \frac{1}{K_L Q_{\max}} + \frac{C_e}{Q_{\max}} \quad (1)$$

where C_e (mg/L) is the equilibrium concentration of nitrate, q_e (mg/g) is the amount of nitrate adsorbed per unit mass of the mat, Q_{\max} (mg/g) is the maximum adsorption capacity, and K_L (L/mg) is the Langmuir constant related to the adsorption binding energy. From the linear plot of C_e/q_e versus C_e , the calculated Q_{\max} was 7.17 mg/g, and the Langmuir constant K_L was determined to be 0.063 L/mg, with a correlation coefficient (r^2) of 0.93. These results indicated that nitrate adsorption primarily occurs as a monolayer on a homogeneous surface. The Freundlich equation, another equilibrium isotherm model that describes adsorption onto heterogeneous surfaces, is expressed by Equation (2) (Santos et al., 2020; Song et al., 2016):

$$\log q_e = \log K_F + \frac{1}{n} \log C_e \quad (2)$$

where K_F $\text{mg/g(L/mg)}^{1/n}$ is the Freundlich constant, indicative of adsorption capacity, and $1/n$ is a Freundlich intensity parameter that represents the adsorption strength. The linear plot of $\log q_e$ versus $\log C_e$ provided a K_F value of 0.79 $\text{mg/g(L/mg)}^{1/n}$ and an n value of 1.9, with a high r^2 value of 0.99. The n value greater than 1 suggests favorable adsorption, while the high r^2 value indicated an excellent fit of the Freundlich model to the experimental data.

The theoretical parameters for both isotherm models are summarized in Table 1. The dual fitting of the data using the Langmuir and Freundlich models demonstrated the ability of the mat to support both homogeneous and heterogeneous adsorption mechanisms. These results suggested that the primary role of the mat in sensing applications was to facilitate nitrate ion transport to the sensor interface without significantly sequestering or obstructing the ions.

3.2. Sensor calibration and characterization

Both the nitrate sensor wrapped with the PVA/PSF-PMMA mat and its bare counterpart were characterized in the laboratory using pre-treated soil samples with varying nitrate concentrations ranging from 10 to 100 mg/kg at a constant soil water content of 0.4 g/g (see Section 2.5 for sample preparation details). Following each measurement, the sensors were rinsed with DI water to remove residual soil and dried with nitrogen before testing the next sample. This procedure was repeated for

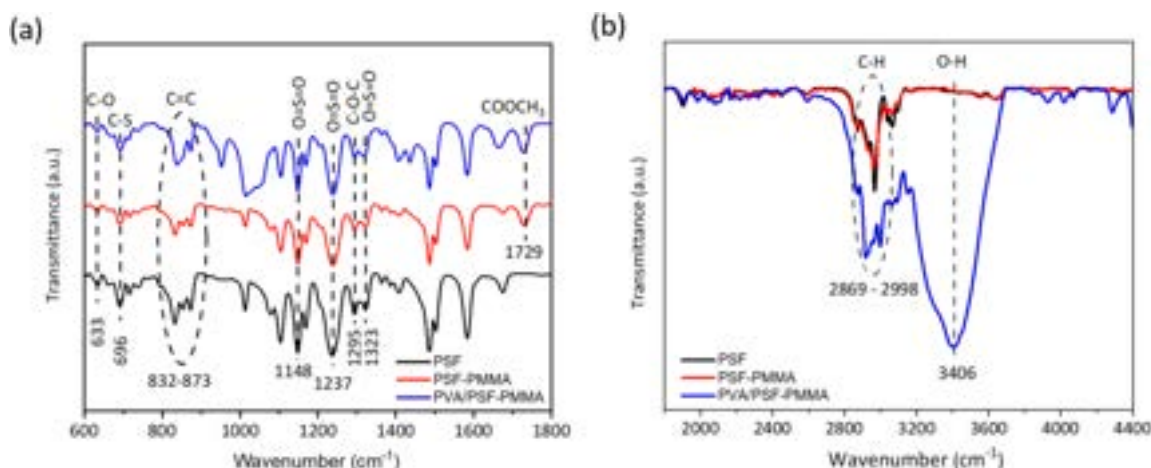


Fig. 3. FTIR spectra of PSF, PSF-PMMA, PVA/PSF-PMMA nanofibers from 600 to 1800 cm^{-1} (a) and from 1800 and 4400 cm^{-1} (b).

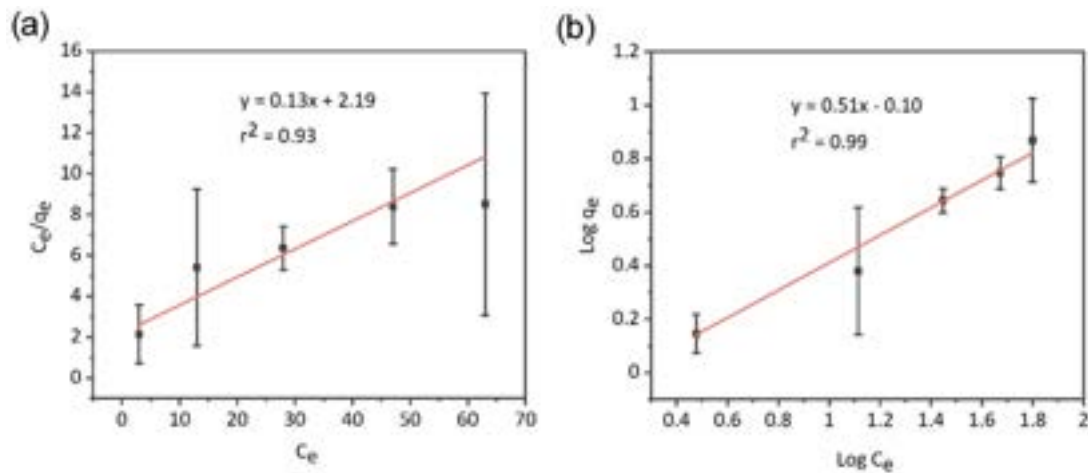


Fig. 4. (a) Langmuir isotherm for monolayer nitrate adsorption on the surface of the PVA/PSF-PMMA nanofibrous mat, showing the relationship between C_e/q_e and C_e . (b) Freundlich isotherm for nitrate adsorption on the surface of the PVA/PSF-PMMA nanofibrous mat, showing the relationship between $\log(q_e)$ and $\log(C_e)$.

Table 1

Isotherm parameters for nitrate ion adsorption onto the PVA/PSF-PMMA mat.

Isotherm model	Parameter	Value
Langmuir	Q_{\max} (mg/g)	7.17
	K_L (L/mg)	0.063
	r^2	0.93
Freundlich	n	1.9
	K_F (mg/g) (L/mg) $^{1/n}$	0.79
	r^2	0.99

five different soil nitrate concentrations. The output voltage signals of both types of sensors significantly changed with increasing concentrations of NO_3^- (Fig. 5a, 5b). Their calibration plots exhibited linear relationships between the output voltage and the logarithmic concentration of NO_3^- (Fig. 5c, 5d). The sensitivity and the correlation coefficient obtained from the calibration plots were found to be -54.93 mV/dec and 0.99, respectively, for the mat-wrapped sensor and -54.24 mV/dec and 0.99 for the bare sensor. Therefore, the PVA/PSF-PMMA nanofibrous mat did not compromise the sensitivity of the sensor to detect nitrate ions. It should be noted that the potential difference between the mat-wrapped sensor and its bare counterpart for the same nitrate concentration might be attributed to the inherent variability in soil media which the ISM of each sensor was exposed.

The reproducibility of the mat-wrapped sensor was evaluated by measuring the NO_3^- concentration (25 mg/kg) in the pretreated soil (see Section 2.5 for sample preparation details), using five identical sensors produced from the same batch. These sensors provided similar calibration curves, with their sensitivities between -52.31 and -56.62 mV/dec (Fig. 5e). The histogram in the inset of Fig. 5e shows the response concentrations of these sensors using their respective calibrations. The relative standard deviation of the measured concentrations across these sensors was $\sim 3\%$, indicating considerable reproducibility of the mat-wrapped sensors.

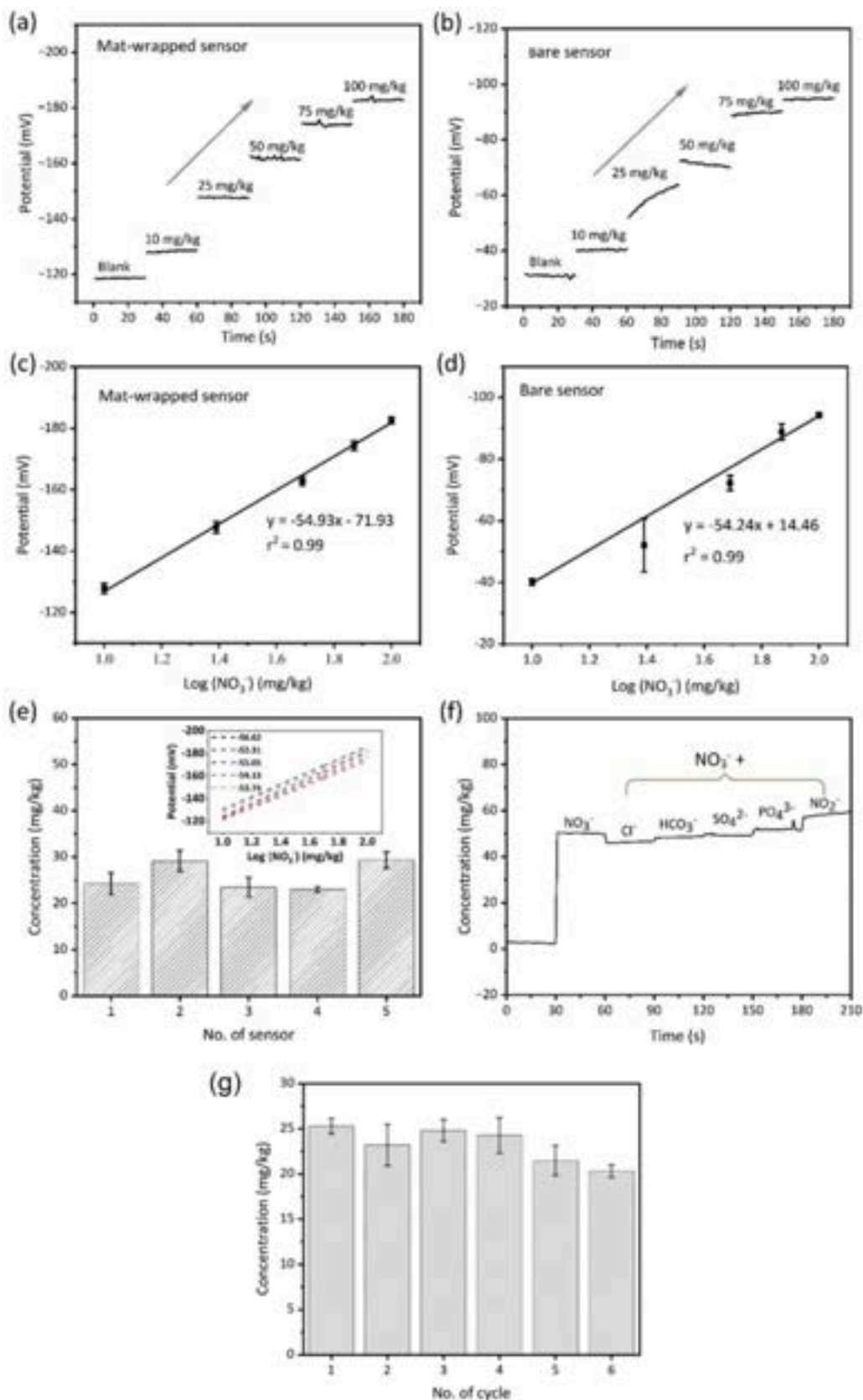
To evaluate the selectivity of the mat-wrapped sensor, various ions were added to soil samples, including 50 mg/kg NO_3^- alone, and mixtures of 50 mg/kg NO_3^- with 50 mg/kg of interference ion (Cl^- , HCO_3^- , SO_4^{2-} , PO_4^{3-} , or NO_2^-) (Fig. 5f). A blank soil sample without any added ions was also tested by the sensor, which indicated negligible (i.e., irrelevant for agricultural decision making) nitrate concentrations of ~ 2 mg/kg. When 50 mg/kg of NO_3^- was added to this blank soil sample, the sensor response increased to ~ 51 mg/kg NO_3^- . The sensor response varied when interference ions were present: it decreased by 8% with 50 mg/kg NO_3^- and 50 mg/kg Cl^- , by 4% with 50 mg/kg NO_3^- and 50 mg/kg HCO_3^- , by 2% with 50 mg/kg NO_3^- and 50 mg/kg SO_4^{2-} , and increased

by 2% with 50 mg/kg NO_3^- and 50 mg/kg PO_4^{3-} . Notably, the response increased by 16% with 50 mg/kg NO_3^- and 50 mg/kg NO_2^- , likely due to the molecular similarity between NO_3^- and NO_2^- .

To evaluate the recyclability of the mat-wrapped sensor, tests were conducted using six soil samples, each containing 25 mg/kg of nitrate at a constant gravimetric soil water content of 0.4 g/g (see Section 2.5 for sample preparation details). After each measurement, the sensor was thoroughly washed with DI water to remove residual soil and nitrate before being reused with the next soil sample. This process was repeated for six cycles, during which the sensor response was monitored to assess its reusability. The histogram in Fig. 5g illustrates the sensor readout of nitrate concentrations across these cycles. The relative standard deviation of the measured concentrations was $\sim 8\%$, demonstrating the good recyclability and consistent performance of the mat-wrapped sensor over multiple uses.

Both mat-wrapped and bare sensors were exposed to a 50 mg/kg NO_3^- concentration at varying soil water contents (0.2–0.4 g/g) in a controlled environment. Each soil container, with a specified soil water content, housed both a mat-wrapped and a bare sensor for 17 days. The lower panel of Fig. 6a shows that at 0.2 g/g water content, the bare sensor exhibited an unstable response during the measurement; this instability was likely due to the limited ability of the sensor to draw soil water to its surface and the influence of charged soil particles on its voltage output. Interestingly, the bare sensor took 4–5 days to reach a relatively stable response at 0.3 g/g of soil water content (the middle panel of Fig. 6a) and only 2–3 days at 0.4 g/g of soil water content (the upper panel of Fig. 6a). These results indicated that higher soil water contents are favorable for the bare sensor to conduct soil nitrate measurements.

In contrast, the mat-wrapped sensor in soil with 0.2 g/g water content exhibited a more consistent response after 2–3 days compared to the bare sensor at the same water content level. At 0.3 g/g water content, the mat-wrapped sensor took 1–2 days to reach a relatively stable voltage output, while at 0.4 g/g water content, the sensor achieved signal stabilization within one day (Fig. 6b). These results suggested that the PVA/PSF-PMMA mat improved the signal stability of the nitrate sensor under varying gravimetric soil water contents. Additionally, the time required for the mat-wrapped sensor to reach a stable response depended on the soil water content level, with higher soil water content levels allowing the sensor to stabilize more quickly by drawing water to its surface. These soil water contents represent the full range of water contents typically observed during early season maize growth when nitrogen fertilizer management decisions are made.



(caption on next page)

Fig. 5. (a, b) Potentiometric response of the mat-wrapped sensor (a) and bare sensor (b) to varying soil nitrate concentrations (10 to 100 mg/kg). (c, d) Calibration plots for the mat-wrapped sensor (c) and bare sensor (d) showing the relationship between the logarithm of nitrate concentrations against output potential responses. Error bars represent the standard deviation from five repetitive experiments. (e) Measured soil nitrate concentrations of five identical sensors exposed to 25 mg/kg of nitrate concentration in soil. Inset: Electrode potential relative to nitrate concentration for five identical sensors in soil. The sensitivity values for each test are displayed as an inset within the plot. (f) Selectivity test of the mat-wrapped soil sensor in the presence of 50 mg/kg NO_3^- alone and 50 mg/kg NO_3^- mixed with 50 mg/kg of one of the interference ions (Cl^- , HCO_3^- , SO_4^{2-} , PO_4^{3-} , and NO_2^-) in soil. (g) Recyclability of the mat-wrapped sensor in soil samples for nitrate detection. The histogram shows the sensor response in six identical soil samples, each containing 25 mg/kg of nitrate. Between cycles, the sensor was rinsed with DI water.

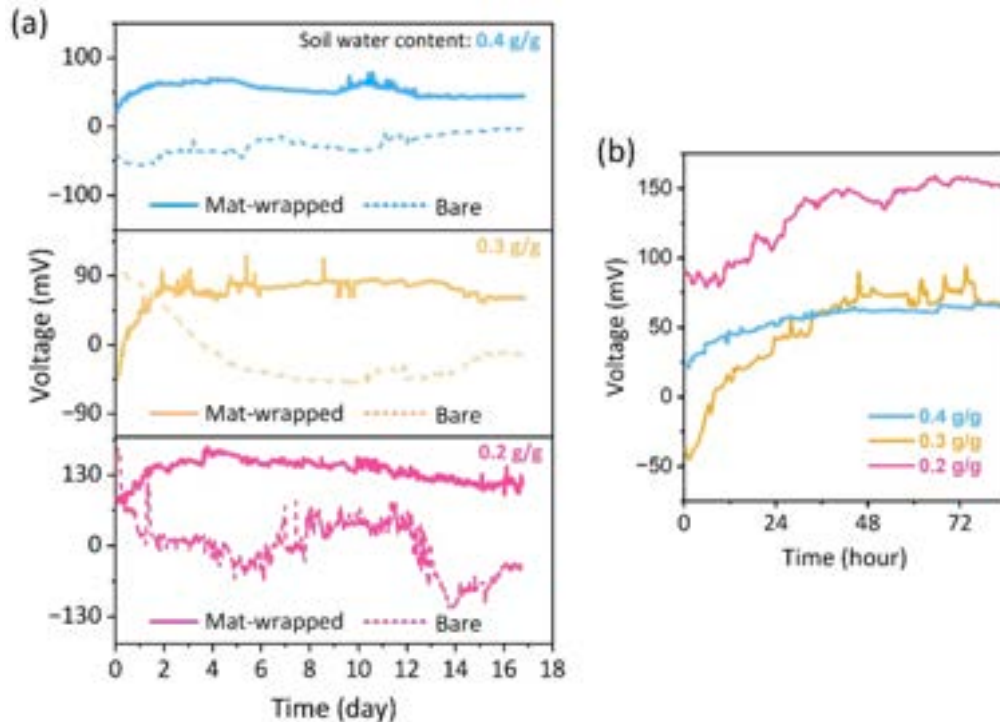


Fig. 6. (a) Voltage outputs from the mat-wrapped (solid line) and bare (dashed line) soil sensors exposed to a constant soil NO_3^- concentration of 50 mg/kg at three gravimetric soil water contents (upper panel: 0.4 g/g; middle panel: 0.3 g/g; lower panel: 0.2 g/g). (b) Zoom-in on the responses of the three mat-wrapped sensors during the first 84 h after installation.

3.3. Field sensing of soil nitrate

The field measurement capabilities of the mat-wrapped and bare soil nitrate sensors were assessed. Details of sensor installation, soil sampling, preparation, and salt extract measurement are provided in Section 2.6. Fig. 7a shows that throughout the 24-day period, the mat-wrapped and bare sensors exhibited similar trends in soil nitrate changes over time. However, the wrapped sensor provided more detailed variations in soil nitrate concentrations than the bare sensor. For example, the wrapped sensor even revealed smaller but clear diurnal changes in soil nitrate concentrations over several days; however, such changes were barely detected by the bare sensor.

To evaluate the accuracy and reliability of the mat-wrapped and bare sensors compared to the salt extract method, linear regression, paired sample *t*-test, and Bland-Altman analyses (Zhu et al., 2021) were performed. Linear regression was used to describe the relationship between sensor outputs (both mat-wrapped and bare) and the salt extract measurements (Fig. 7b). The coefficient of determination (r^2) quantified the variance in the dependent variable (sensor output on the y-axis) explained by the independent variable (salt-extract data on the x-axis). The sensor data represented mean daily soil NO_3^- concentration on the sampling days: 9/20, 9/24, 9/28, 10/2, 10/6, and 10/9. The regression line for the mat-wrapped sensor was characterized by the equation $y = 0.633x + 4.380$ with an r^2 value of 0.944, indicating a strong correlation between the mat-wrapped sensor measurements and the salt extract method. The slope of 0.633 indicated that this sensor tended to

underreport nitrate levels as compared to the conventional method. In contrast, the bare sensor data followed the equation $y = 0.735x - 5.923$ with an r^2 value of 0.821. While the r^2 value of the bare sensor indicated a reasonable correlation, it was lower than that of the mat-wrapped sensor. The 1:1 line in Fig. 7b represented the ideal match between the sensor and salt extract measurements, but the actual slopes of both regression lines were below 1. This discrepancy arose from the different approaches used to assess soil NO_3^- concentration in different nitrogen pools. The salt extract method estimated the bioavailable nitrogen pool (including both inorganic and organic forms), while the sensors measured mobile nitrate ions in the soil pore water.

The paired sample *t*-tests revealed statistically significant differences between both sensor measurements and the salt extract method ($p < 0.001$) (Fig. 7b). The *t*-statistics, which represented the difference between sample means divided by the standard error of the difference, provided insight into the magnitude of the differences. A higher *t*-statistic reflected a larger discrepancy, while a lower value suggested closer agreement. Notably, the mat-wrapped sensor exhibited a lower *t*-statistic ($t = 6.92$) compared to the bare sensor ($t = 12.64$), indicating closer alignment with the salt extract method. The confidence interval (CI) complemented the *t*-test by providing a range where the true parameter (e.g., mean difference) is estimated to lie at a given confidence level (e.g., 95%). A narrower CI indicates greater precision in the estimate. The mat-wrapped sensor exhibited a narrower CI (4.9 to 9.47 mg/kg) compared to the bare sensor (11.83 to 16.81 mg/kg), indicating reduced variability and improved measurement consistency. The CI was

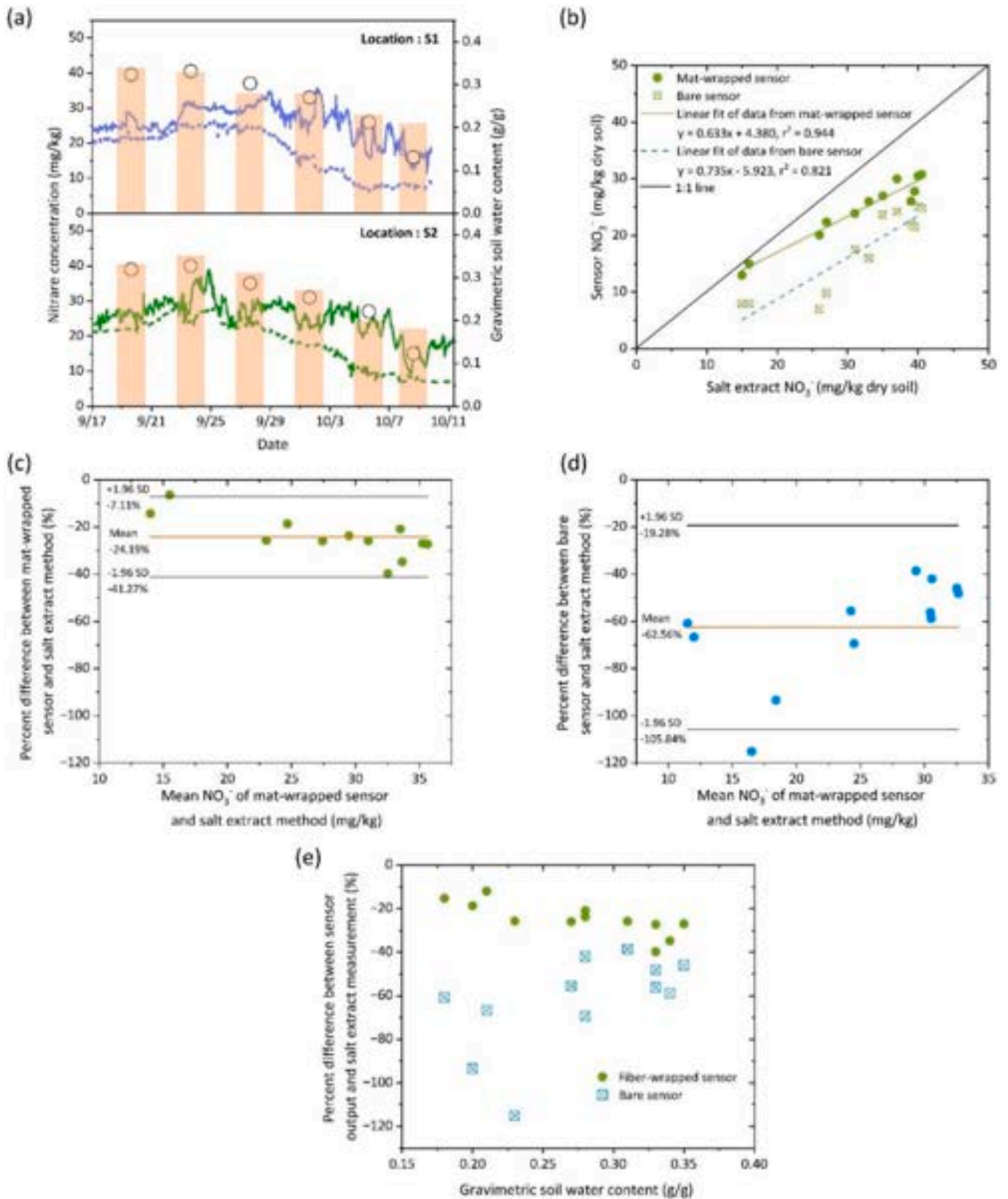


Fig. 7. (a) Soil nitrate concentrations measured with mat-wrapped sensors (continuous solid lines), bare sensors (continuous short-dash lines), and salt extract methods (discrete black circles) at two close locations (40 cm apart) in the field. The corresponding gravimetric soil water contents (g/g) of the soil samples used in the salt extract method are also shown (brown columns). (b) Soil nitrate concentration measured with the sensor and salt extraction methods in the field experiment described in (a). Sensor data represent the mean daily soil nitrate concentration on the day of soil sampling and salt extraction. The solid black line of equality is shown for reference. (c, d) Bland-Altman plots showing percentage differences between salt extract and sensor measurements against the mean of the two measurements. Mat-wrapped sensors are shown in (c), and bare sensors are shown in (d). The brown horizontal line indicates the mean difference between methods, and the black horizontal lines indicate 95 % confidence intervals. (e) Percentage differences between salt extract and sensor (both mat-wrapped and bare) measurements against gravimetric soil water content.

calculated from the sample mean, standard error, and a t-value corresponding to the desired confidence level and degrees of freedom.

Moreover, the Bland-Altman analysis assessed the agreement between the salt extract and sensor (both wrapped and unwrapped) measurement data from Fig. 7b against the mean of these two measurements. The Bland-Altman plot (Fig. 7c) showed that the mean percentage difference between the bare sensor and the salt extract method was -62.56% , indicating a substantial underestimation of nitrate levels by the bare sensor compared to the conventional method. The limits of agreement were calculated at -19.28% (upper limit, $+1.96$ SD; SD means standard deviation) and -105.84% (lower limit, -1.96 SD). The scatter of data points around the mean highlighted a consistent negative bias, with most points falling below the mean percentage difference. In contrast, the Bland-Altman plot for the mat-wrapped sensor (Fig. 7d) displayed a mean percentage difference of -24.19% , indicating a closer approximation to the conventional method compared to the bare sensor. The limits of agreement were narrower, with the upper limit at -7.11% and the lower limit at -41.27% . The data points for the mat-wrapped sensor were more tightly clustered around the mean, suggesting higher consistency and less variability in the measurements. The comparative analysis of the mat-wrapped and bare sensors revealed that the former outperformed the latter in terms of measurement reliability and consistency.

The uncertainty of the sensor measurement was analyzed across varying soil moisture levels. Fig. 7e illustrates the percentage difference between the sensor and the salt extract method across various gravimetric soil water contents. For the mat-wrapped sensor, the percentage differences were relatively stable across a range of soil water contents from 0.15 to 0.40 g/g. This sensor consistently showed a percentage difference of around -20% , indicating a relatively constant underestimation of nitrate levels compared to the conventional method. This stability suggested that the mat-wrapped sensor was less affected by varying soil moisture levels, providing reliable measurements under different soil moisture conditions. In contrast, the bare sensor exhibited a wider range of percentage differences, ranging from -120% to -40% . The data points for the bare sensor showed significant variability,

particularly at lower soil water contents (0.15 to 0.25 g/g), where the percentage differences were more pronounced and erratic. This indicated that the accuracy of the bare sensor was highly influenced by soil moisture levels, especially in drier soil conditions.

Potential sources of error and uncertainty in sensor measurements include soil water content levels, interference from non-target ions, material degradation, surface charges on soil particles, and environmental impacts. Low soil water content can hinder ion mobility, reducing the efficiency of ion transport to the sensor surface. For instance, bare sensors exhibited unstable signal outputs under low soil water conditions (Fig. 6a). Additionally, charged soil particles may induce voltage fluctuations, contributing to measurement inconsistencies. Interference from non-target ions, such as Cl^- , K^+ , and PO_4^{3-} , is another significant source of uncertainty, as shown in the selectivity tests (Fig. 5f). While the mat-wrapped sensor mitigates some of these issues by promoting stable interaction with the soil solution, challenges remain due to factors such as material durability and interference ions.

A variety of low-cost nitrate sensing technologies have been reported, utilizing different detection mechanisms and materials, with varying levels of success in laboratory and field environments (Table 2). While many sensors performed well in controlled laboratory conditions, their application in field settings remains limited, particularly for soil nitrate monitoring. The ISE-based sensor presented in this study, enhanced with a PVA/PSF-PMMA nanofibrous mat, demonstrated effective soil nitrate monitoring across varying soil water content levels under both laboratory and field conditions over extended periods. Several other ISE sensors have also incorporated water-absorbing materials, such as PVDF and hydrogel, to improve interaction with soil; however, their testing was limited to laboratory settings. For example, hydrogel-coated ISE sensors showed stable performance for 14 days in lab conditions (Fan et al., 2022), and the PVDF-coated ISE sensors demonstrated reliable operation in laboratory soil tests (Chen et al., 2024). But, their suitability for field applications has yet to be evaluated. Enzymatic and microfluidic sensors were also explored for nitrate detection (Xu et al., 2017). However, enzyme stability and the

Table 2
Performance comparisons of different nitrate sensors under laboratory and field-testing conditions.

Sensing method	Water absorber	Sensitivity	Dynamic range (mg/L)	Testing samples	Lab test period	Field test period	References
ISE	NA	NA	10 – 1000	Soil (loam)	Several hours	73 days	(Zhu et al., 2021)
ISE	PVDF	56.3 mV/decade	10 – 200	Soil (sandy)	Several hours	NA	(Chen et al., 2024)
ISE	NA	64 mV/decade	1 – 1500	Soil (loam)	25 days	NA	(Ali et al., 2019)
ISE	Hydrogel	30.6 mV/decade	1 – 128	Soil (sandy loam)	14 days	NA	(Fan et al., 2022)
ISE	NA	54.1 mV/decade	3.1 – 1240	Soil (peat)	1 day	Several hours	(Baumbauer et al., 2022)
ISE	NA	58 mV/decade	1 – 64	Wastewater	24 days	NA	(Fan et al., 2020)
ISE	NA	51.7 mV/decade	0.62 – 6200	Soil	1 day	NA	(Garland et al., 2018)
ISE	NA	51.61 mV/decade	6.2 – 248	Fertilizers	2500 sec	NA	(Chanam et al., 2016)
ISE	NA	NA	0.0062 – 6200	Synthetic water sample	60 sec	NA	(Paczosa-Bator, 2014)
Microfluidic electrophoresis	Ceramic tube	0.0915 mV/ μM	1.24 – 6.2	Soil (loam)	300 sec	NA	(Xu et al., 2017)
Ion-sensitive transistor	NA	28 mV/decade	10^{-7} – 100	Tap and snow water	12 min	NA	(Xu et al., 2024)
Non-enzymatic, electrochemical	Extraction filter	NA	3.1 – 310L	Soil	32 days	Several hours	(Chen et al., 2023)
Non-enzymatic, electrochemical	NA	0.38 $\mu\text{A}/\text{mM}$	0.07 – 100	River, lake, tap water	7 days	NA	(Wei et al., 2024)
Fiber optic	NA	0.16 $\mu\text{W}/\text{ppm}$	0.2 – 40	Synthetic water sample	21 days	NA	(Shahnia et al., 2020)
Optical absorption spectroscopy	NA	1.4 L/mg	0 – 1.4	Synthetic water sample	300 sec	NA	(Lu et al., 2025)
Mach-Zehnder interferometer	NA	15 pM/ppm	0 – 100	Synthetic water sample	150 sec	NA	(Noman et al., 2022)
ISE	Fiber mat	54.93 mV/decade	10 – 100	Soil (loam)	17 days	24 days	This work

complexity of microfluidic settings posed challenges for field use. Non-enzymatic sensors, such as those using differential-pulsed voltammetry or absorption modules, simplified the detection process but required further testing to establish their reliability for field applications (Lu et al., 2025). While fiber-optic sensors, field-effect transistors, and spectrophotometric methods offered high precision in nitrate detection, they were often limited by their bulky designs and the need for frequent recalibration (Noman et al., 2022; Xu et al., 2024; Rudd et al., 2017). These limitations reduced their practicality for dynamic and long-term field environments. Our sensor coated with the PVA/PSF-PMMA mat showed promise as a practical, inexpensive solution for soil nitrate monitoring under field conditions.

4. Conclusions

We developed a water-absorbing nanofibrous mat for use in ISE-based soil nitrate sensors. This polymeric mat, composed of PVA, PMMA, and PSF, was fabricated using electrospinning and electrospray techniques. The mat was wrapped around the sensor to draw soil water onto the sensor surface, maintaining a wet state that facilitated the interaction of soil water ions with the sensor. This design addresses a critical issue faced by many existing soil sensors: the lack of water-absorbing mechanisms for interacting with soil solutions in relatively dry conditions.

Linear regression analysis of the field measurement results revealed that the mat-wrapped nitrate sensor had a stronger correlation with the salt extract method compared to the bare sensor. This improvement was likely due to the ability of the mat to enhance the presence of soil water and ions at the sensor surface, enabling more representative measurements of soil nitrate levels similar to the conventional method, which analyzed large, homogenized samples. The Bland-Altman analysis revealed that the mat-wrapped sensor exhibited a smaller mean bias and narrower limits of agreement compared to the bare sensor, indicating closer alignment with the conventional salt extract method. Additionally, paired sample t-tests confirmed that the mat-wrapped sensor exhibited improved consistency and lower variability relative to the bare sensor when compared to the conventional method.

Furthermore, the mat-wrapped sensor performed consistently across varying soil moisture conditions, maintaining a consistent percentage difference with the salt extract method. In contrast, the bare sensor measurements were compromised by changes in soil water content, showing greater variability and less reliability. These findings suggest the mat-wrapped sensor is well-suited for consistent nitrate monitoring across a range of soil moisture levels representative of typical environmental conditions, making it a more viable alternative for robust field applications compared to the bare sensor.

However, the long-term stability and durability of the mat-wrapped sensor under field conditions remain areas requiring further investigation, particularly regarding microbial activity, wet-dry cycles, soil abrasion, and biodegradability. Deployment in heterogeneous soil environments poses additional challenges, including maintaining consistent sensor-soil particle contact and ensuring uniform water infiltration through the mat. Optimizing the material properties of the nanofibrous mat is critical to enhancing its structural integrity and water-absorbing capacity, thereby improving its effectiveness under field conditions. The biodegradability of the materials used in the mat remains a concern for environmental sustainability. While PVA is partially biodegradable, PSF and PMMA are synthetic polymers with limited degradation in natural environments. Future efforts should focus on integrating bio-based or fully biodegradable materials into the sensor design, ensuring that the hydrophilic properties, mechanical durability, and ion transport efficiency are maintained without compromising performance. Addressing these challenges will necessitate extensive research, involving both controlled experiments and field trials across diverse environmental settings.

From a system integration perspective, we will focus on integrating

the mat-wrapped soil nitrate sensor with soil moisture or water potential sensors, along with energy harvesting technologies (Jiang et al., 2022), to improve accuracy, reliability, and longevity for long-term field monitoring. Soil water content significantly affects nitrate sensor readings. Since nitrate ions are highly soluble in water, they move more freely within the soil when moisture levels are higher, leading to a more uniform distribution and easier detection by sensors. In contrast, during dry conditions, nitrate ions may become less mobile and trapped in isolated water films, making them harder to detect and potentially causing inaccurate estimations of nitrate levels. By integrating soil moisture (or water potential) measurements with nitrate monitoring, these variations can be accounted for, resulting in more reliable and consistent detection of soil nitrate levels. Additionally, combining these measurements with subsoil nitrous oxide sensors, which monitor emissions of a potent greenhouse gas (Reay et al., 2012) will enhance our understanding of soil microbial processes. This integration will provide valuable insights into the interactions between nitrogen availability for plants and nitrous oxide production, supporting the development of more sustainable agricultural practices that balance productivity with environmental stewardship.

CRediT authorship contribution statement

Vignesh Kumar Thoomatti Haridass: Writing – review & editing, Writing – original draft, Validation, Software, Methodology, Investigation, Formal analysis, Data curation. **Michael J Castellano:** Writing – review & editing, Investigation. **Liang Dong:** Writing – review & editing, Visualization, Supervision, Resources, Project administration, Methodology, Investigation, Funding acquisition, Formal analysis, Data curation, Conceptualization.

Declaration of competing interest

The authors declare the following financial interests/personal relationships which may be considered as potential competing interests: [Liang Dong reports financial support was provided by National Science Foundation. Liang Dong reports financial support was provided by US Department of Agriculture. Michael J. Castellano reports financial support was provided by National Science Foundation. Michael J. Castellano reports financial support was provided by US Department of Agriculture. Liang Dong reports a relationship with EnGeniousAg, LLC (Ames, IA, USA) that includes: equity or stocks. Michael Castellano reports a relationship with EnGeniousAg, LLC (Ames, IA, USA) that includes: equity or stocks. Michael Castellano reports a relationship with CropX Technologies Ltd. that includes: consulting or advisory. Liang Dong and Michael Castellano have patents licensed to EnGeniousAg, LLC. The authors declare the following competing financial interest: EnGeniousAg LLC had a license from the Iowa State University Research Foundation to use the ISE sensor technology (excluding nanofiber coating) and described in Reference Ali et al., 2019. L.D. and M.J.C. had equity in EnGeniousAg, which was acquired by CropX Technologies Ltd. If there are other authors, they declare that they have no known competing financial interests or personal relationships that could have appeared to influence the work reported in this paper].

Acknowledgments

This work was supported in part by the Plant Sciences Institute at Iowa State University; in part by the U.S. Department of Agriculture - National Institute of Food and Agriculture (USDA-NIFA) under grant numbers 2020-67021-31528 and 2022-67019-38686; in part by the U.S. National Science Foundation under grant numbers 2316481 and 2125484; in part by the AI Research Institutes program supported by NSF and USDA-NIFA under AI Institute for Resilient Agriculture under grant number 2021-67021-35329.

Data availability

Data will be made available on request.

References

- Ahmad, R., Bhat, K.S., Ahn, M.-S., Hahn, Y.-B., 2017. Fabrication of a robust and highly sensitive nitrate biosensor based on directly grown zinc oxide nanorods on a silver electrode. *New J. Chem.* 41, 10992–10997.
- Ali, M.A., Wang, X., Chen, Y., Jiao, Y., Mahal, N.K., Moru, S., Castellano, M.J., Schnable, J.C., Schnable, P.S., Dong, L., 2019. Continuous monitoring of soil nitrate using a miniature sensor with poly (3-octyl-thiophene) and molybdenum disulfide nanocomposite. *ACS Appl. Mater. Interfaces* 11, 29195–29206.
- Baumbauer, C.L., Goodrich, P.J., Payne, M.E., Anthony, T., Beckstoffer, C., Toor, A., Silver, W., Arias, A.C., 2022. Printed potentiometric nitrate sensors for use in soil. *Sensors* 22, 4095.
- Bieg, C., Fuchsberger, K., Stelzle, M., 2017. Introduction to polymer-based solid-contact ion-selective electrodes—basic concepts, practical considerations, and current research topics. *Anal. Bioanal. Chem.* 409, 45–61.
- Bowles, T.M., Atallah, S.S., Campbell, E.E., Gaudin, A.C.M., Wieder, W.R., Grandy, A.S., 2018. Addressing agricultural nitrogen losses in a changing climate. *Nat Sustain* 1, 399–408.
- Chanam, S., Taweetong, W., Kaewyai, K., Thienwong, P., Takaew, A., Chaisuksant, R., 2016. Fabrication of a nitrate selective electrode for determination of nitrate in fertilizers by using flow injection analysis system. *Procedia Chem.* 20, 73–75.
- Chee, T.Y., Yusoff, A.R.M., Abdullah, F., Mahmood, W.M.A.W., Jasni, M.J.F., Malek, N.A. N.N., Buang, N.A., Govarthanan, M., 2022. Fabrication, characterization and application of electrospun polysulfone membrane for phosphate ion removal in real samples. *Chemosphere* 303, 135228.
- Chen, K.-Y., Biswas, A., Cai, S., Huang, J., Andrews, J., 2024. Inkjet printed potentiometric sensors for nitrate detection directly in soil enabled by a hydrophilic passivation layer. *Adv. Mater. Technol.* 9, 2301140.
- Chen, Y., Tang, Z., Zhu, Y., Castellano, M.J., Dong, L., 2021. Miniature multi-ion sensor integrated with artificial neural network. *IEEE Sens. J.* 21, 25606–25615.
- Essoussi, H., Barhoumi, H., Bibani, M., Ktari, N., Wendler, F., Al-Hamry, A., Kanoun, O., 2019. Ion-imprinted electrochemical sensor based on copper nanoparticles-polyaniline matrix for nitrate detection. *J Sens* 2019, 4257125.
- Fan, Y., Huang, Y., Linthicum, W., Liu, F., Beringsh, A.O., Dang, Y., Xu, Z., Chang, S.-Y., Ling, J., Huey, B.D., 2020. Toward long-term accurate and continuous monitoring of nitrate in wastewater using poly (tetrafluoroethylene)(PTFE)-solid-state ion-selective electrodes (S-ISEs). *ACS Sens* 5, 3182–3193.
- Fan, Y., Wang, X., Qian, X., Dixit, A., Herman, B., Lei, Y., McCutcheon, J., Li, B., 2022. Enhancing the understanding of soil nitrogen fate using a 3D-electrospray sensor roll casted with a thin-layer hydrogel. *Environ. Sci. Tech.* 56, 4905–4914.
- Garland, N.T., McLamore, E.S., Cavallaro, N.D., Mendivelso-Perez, D., Smith, E.A., Jing, D., Claussen, J.C., 2018. Flexible laser-induced graphene for nitrogen sensing in soil. *ACS Appl. Mater. Interfaces* 10, 39124–39133.
- Hack, H.R.B., 1984. Calculation of the field volumetric water content of cracking clay soils from measurements of gravimetric water content and bulk density. *J. Soil Sci.* 35, 299–315.
- Hu, J., Stein, A., Bühlmann, P., 2016. Rational design of all-solid-state ion-selective electrodes and reference electrodes. *TRAC Trends Anal. Chem.* 76, 102–114.
- Hu, L., Chee, P.L., Sugiarto, S., Yu, Y., Shi, C., Yan, R., Yao, Z., Shi, X., Zhi, J., Kai, D., Yu, H.-D., Huang, W., 2023. Hydrogel-based flexible electronics. *Adv. Mater.* 35, 2205326.
- Huang, S., Mansouri, J., Le-Clech, P., Leslie, G., Tang, C.Y., Fane, A.G., 2022. A comprehensive review of electrospray technique for membrane development: Current status, challenges, and opportunities. *J Memb Sci* 646, 120248.
- Jackson, D.T., Nelson, P.N., 2019. Preparation and properties of some ion selective membranes: A review. *J. Mol. Struct.* 1182, 241–259.
- Jiang, H., Halverson, L.J., Dong, L., 2022. A miniaturized bioelectricity generation device using plant root exudates to feed electrogenic bacteria. *Sens. Actuators, A* 342, 113649.
- Khanfar, M.F., Al-Faqheri, W., Al-Halhouli, A., 2017. Low cost lab on chip for the colorimetric detection of nitrate in mineral water products. *Sensors* 17, 2345.
- Kung, C.-T., Hou, C.-Y., Wang, Y.-N., Fu, L.-M., 2019. Microfluidic paper-based analytical devices for environmental analysis of soil, air, ecology and river water. *Sens Actuators B Chem* 301, 126855.
- Li, M., Li, J., Zhou, M., Xian, Y., Shui, Y., Wu, M., Yao, Y., 2020. Super-hydrophilic electrospun PVDF/PVA-blended nanofiber membrane for microfiltration with ultrahigh water flux. *J. Appl. Polym. Sci.* 137, 48416.
- Lu, L., Zhao, R., Chen, H., Tan, L., Chen, D., Liu, L., Xi, J., 2025. An optical sensor for in situ real-time detection of intermediate products in nitrate reduction reactions. *J Mater Chem A, Advanced Article*.
- Mohammad, N., Atassi, Y., 2020. Adsorption of methylene blue onto electrospun nanofibrous membranes of polylactic acid and polyacrylonitrile coated with chloride doped polyaniline. *Sci. Rep.* 10, 13412.
- Murphy, B.J., Luy, E.A., Panzica, K.L., Johnson, G., Sieben, V.J., 2021. An Energy efficient thermally regulated optical spectroscopy cell for lab-on-chip devices: Applied to nitrate detection. *Micromachines* 12, 861.
- Noman, A.A., Dash, J.N., Cheng, X., Tam, H.-Y., Yu, C., 2022. Mach-Zehnder interferometer based fiber-optic nitrate sensor. *Opt. Express* 30, 38966–38974.
- Obaid, M., Barakat, N.A.M., Fadali, O.A., Motlak, M., Almajid, A.A., Khalil, K.A., 2015. Effective and reusable oil/water separation membranes based on modified polysulfone electrospun nanofiber mats. *Chem. Eng. J.* 259, 449–456.
- Paczosa-Bator, B., 2014. Effects of type of nanosized carbon black on the performance of an all-solid-state potentiometric electrode for nitrate. *Microchim. Acta* 181, 1093–1099.
- Park, M.J., Gonzales, R.R., Abdel-Wahab, A., Phuntsho, S., Shon, H.K., 2018. Hydrophilic polyvinyl alcohol coating on hydrophobic electrospun nanofiber membrane for high-performance thin film composite forward osmosis membrane. *Desalination* 426, 50–59.
- Reay, D.S., Davidson, E.A., Smith, K.A., Smith, P., Melillo, J.M., Dentener, F., Crutzen, P. J., 2012. Global agriculture and nitrous oxide emissions. *Nat. Clim. Chang.* 2 (6), 410–416.
- Rudd, S., Dalton, M., Buss, P., Treijs, A., Portmann, M., Ktoris, N., Evans, D., 2017. Selective uptake and sensing of nitrate in poly (3, 4-ethylenedioxythiophene). *Sci. Rep.* 7, 16581.
- Sadare, O.O., Daramola, M.O., 2021. Blended polysulfone/polyethersulfone (PSF/PES) membrane with enhanced antifouling property for separation of succinate from organic acids from fermentation broth. *ACS Sustain. Chem. Eng.* 9, 13068–13083.
- Santos, L.C., da Silva, A.F., dos Santos Lins, P.V., da Silva Duarte, J.L., Ide, A.H., Meili, L., 2020. Mg-Fe layered double hydroxide with chloride intercalated: synthesis, characterization and application for efficient nitrate removal. *Environ. Sci. Pollut. Res.* 27, 5890–5900.
- Shahnia, S., Ebendorff-Heidepriem, H., Evans, D., Afshar, S., 2020. A fibre-optic platform for sensing nitrate using conducting polymers. *Sensors* 21, 138.
- Shishkanova, T.V., Broncova, G., Kronak, M., Sykora, D., Kral, V., 2011. Important aspects influencing stability of the electrochemical potential of conductive polymer-based electrodes. *J. Mater. Sci.* 46, 7594–7602.
- Sim, S.S.G., Wang, Q., Kentish, S.E., Chen, G.Q., 2023. Equilibrium sorption of monovalent and divalent organic ions in anion exchange membranes. *Ind. Eng. Chem. Res.* 62, 20352–20359.
- Song, W., Gao, B., Xu, X., Wang, F., Xue, N., Sun, S., Song, W., Jia, R., 2016. Adsorption of nitrate from aqueous solution by magnetic amine-crosslinked biopolymer based corn stalk and its chemical regeneration property. *J. Hazard. Mater.* 304, 280–290.
- Sookhankian, M., Mat Teridi, M.A., Tong, G.B., Woi, P.M., Khalil, M., Alias, Y., 2021. Reduced graphene oxide/copper nanoparticle composites as electrochemical sensor materials for nitrate detection. *ACS Appl. Nano Mater.* 4, 12737–12744.
- Sun, X., Agate, S., Salem, K.S., Lucia, L., Pal, L., 2020. Hydrogel-based sensor networks: Compositions, properties, and applications—A review. *ACS Appl. Bio Mater.* 4, 140–162.
- Szigeti, Z., Vigassy, T., Bakker, E., Pretsch, E., 2006. Approaches to improving the lower detection limit of polymeric membrane ion-selective electrodes. *Electroanalysis* 18, 1254–1265.
- Valdés, C., Valdés, O., Bustos, D., Abril, D., Cabrera-Barjas, G., Pereira, A., Villaseñor, J., Polo-Cuadrado, E., Carreño, G., Durán-Lara, E.F., Marican, A., 2021. Use of poly (vinyl alcohol)-malic acid (CLHPMA) hydrogels and chitosan coated calcium alginate (CCCA) microparticles as potential sorbent phases for the extraction and quantitative determination of pesticides from aqueous solutions. *Polymers* 13, 3993.
- Wang, X., Liu, Y., Cheng, H., Ouyang, X., 2022. Surface wettability for skin-interfaced sensors and devices. *Adv. Funct. Mater.* 32, 2200260.
- Wei, S., Xiao, D., Bian, C., Li, Y., 2024. Phosphate and nitrate electrochemical sensor based on a bifunctional boron-doped diamond electrode. *ACS Omega* 9, 20293–20303.
- Wu, H., Shi, J., Ning, X., Long, Y.-Z., Zheng, J., 2022. The high flux of Superhydrophilic-superhydrophobic Janus membrane of cPVA-PVDF/PMMA/GO by layer-by-layer electrospinning for high efficiency oil-water separation. *Polymers* 14, 621.
- Xu, W., Hu, X., Zhuang, S., Wang, Y., Li, X., Zhou, L., Zhu, S., Zhu, J., 2018. Flexible and Salt resistant janus absorbers by electrospinning for stable and efficient solar desalination. *Adv. Energy Mater.* 8, 1702884.
- Xu, Y., Zhou, P., Simon, T., Cui, T., 2024. Ultra-sensitive nitrate-ion detection via transconductance-enhanced graphene ion-sensitive field-effect transistors. *Microsyst. Nanoeng.* 10, 137.
- Xu, Z., Wang, X., Weber, R.J., Kumar, R., Dong, L., 2017. Nutrient sensing using chip scale electrophoresis and in situ soil solution extraction. *IEEE Sens. J.* 17, 4330–4339.
- Zdrachek, E., Bakker, E., 2018. Potentiometric sensing. *Anal. Chem.* 91, 2–26.
- Zhu, Y., Chen, Y., Ali, M.A., Dong, L., Wang, X., Archontoulis, S.V., Schnable, J.C., Castellano, M.J., 2021. Continuous in situ soil nitrate sensors: The importance of high-resolution measurements across time and a comparison with salt extraction-based methods. *Soil Sci. Soc. Am. J.* 85, 677–690.